

Thermal rectification in carbon nanotube intramolecular junctions: Molecular dynamics calculations

Gang Wu*

*Department of Physics and Centre for Computational Science and Engineering,
National University of Singapore, Singapore 117542-76, Republic of Singapore*

Baowen Li†

*Department of Physics and Centre for Computational Science and Engineering,
National University of Singapore, Singapore 117542-76, Republic of Singapore and
NUS Graduate School for Integrative Sciences and Engineering, Singapore 117597, Republic of Singapore*

(Dated: November 29, 2018)

We study heat conduction in $(n, 0)/(2n, 0)$ intramolecular junctions by using molecular dynamics method. It is found that the heat conduction is asymmetric, namely, heat transports preferably in one direction. This phenomenon is also called thermal rectification. The rectification is weakly dependent on the detailed structure of connection part, but is strongly dependent on the temperature gradient. We also study the effect of the tube radius and intramolecular junction length on the rectification. Our study shows that the tensile stress can increase rectification. The physical mechanism of the rectification is explained.

PACS numbers: 66.70.+f, 44.10.+i, 61.46.Fg, 65.80.+n

I. INTRODUCTION

In past two decades, the study of heat conduction in low dimensional model systems has enriched our understanding on heat conduction from microscopic point of view¹. In turn, the study has also lead to some interesting inventions for heat control and management devices. For example, the heat conduction in nonlinear lattice models^{2,3,4} demonstrates rectification phenomenon, namely, heat flux can flow preferably in one direction. Furthermore, the *negative differential thermal resistance* is also found and based on which, a thermal transistor model has been constructed.⁶ Most recently, the two segment model of thermal rectifier proposed in Ref 2,3 has been experimentally realized by using gradual mass-loaded carbon and boron nitride nanotubes.⁷ These works have opened a new era for heat management and heat control in microscopic level.

On the other hand, there have been increasing studies on heat conduction in real nano scale systems⁸. For example, the thermal conduction of single walled carbon nanotubes (SWCNTs) has attracted both theoretical^{9,10,11,12,13,14,15,16,17,18} and experimental^{19,20,21,22,23,24,25} attentions. Almost all experiments and numerical simulations have payed their attention to the extremely high thermal conductivity of SWCNTs. The dependence of the thermal conductivity on the length or chirality of SWCNTs is also extensively studied theoretically. Therefore, one may asks, how can we make heat controlling devices, i.e., the thermal diode or the thermal transistor, from SWCNTs and their derivatives?

In the practical applications, SWCNTs may have many kinds of impurities such as element impurities, isotopic impurities²⁶, topological impurities, etc. Among these numerous derivatives of SWCNTs, the

SWCNT intramolecular junctions (IMJs), which are formed by introducing the pentagon-heptagon rings in SWCNTs, have been expected to be an important structure in the applications. It is well-known that the electronic properties of the SWCNT IMJs have a close relationship with their geometrical or topological characteristics.^{27,28,29,30,31,32,33,34} It is reasonable that the thermal transport behavior of SWCNT IMJs can also be altered by their geometrical characteristics. Compared with the electronic properties, the thermal transport behavior may have not so close relationship with the detailed local geometrical arrangements because it is mainly influenced by the long wavelength phonons. But the non-equilibrium thermal transport behavior of IMJs can be affected by the high-frequency optical phonon modes,³⁵ which can reflect the information of the local defects. So it is interesting to investigate the non-equilibrium thermal transport of different SWCNT IMJs.

In this work, the thermal rectification in $(n, 0)/(2n, 0)$ IMJs and its dependencies on tube radius, IMJ length, and external stress, e.g., tensile and torsional stress are studied. A complex structure of ‘peapod’ structure and IMJ is also studied to investigate the effect of periodical potential on the thermal rectification.

The paper is organized as the follows. In Sec. II we introduce the basic structure of $(n, 0)/(2n, 0)$ IMJ and our numerical method. In Sec. III, the main numerical results are discussed. In Sec IV, we show that the external stress can improve the rectification. In the same section we also show the results of $(n, 0)/C_{60}@/(2n, 0)$ structures, which can be regarded as a combination of peapod structures and $(n, 0)/(2n, 0)$ IMJs. In Sec. V, we give some concluding remarks.

II. MODEL AND METHODOLOGY

A typical $(n, 0)/(2n, 0)$ IMJ structure is depicted in Fig. 1, in which the index n equals to 8. The structure contains two parts, namely, a segment of $(n, 0)$ SWCNT and a segment of $(2n, 0)$ SWCNT. For simplicity, the lengths of the two segments are almost equal in our calculations. The two segments are connected by m pairs of pentagon-heptagon defects. Because $(n, 0)$ and $(2n, 0)$ tubes have the common rotational symmetry C_{2n} , thus when n can be divided exactly by m , we can adjust the defects to make the two segments connect straightly. Especially, if $m = n$, the pentagon-heptagon defects can be arranged in the connection part so that the rotational symmetry of the IMJ is C_n . On the other hand, it is necessary to define a basic system length because the thermal conductivity depends on the system length.²⁶ After setting the lengths of $(n, 0)$ and $(2n, 0)$ tubes to be the same, we can define a basic total length L_0 when both of the two segments contain 24 periods. All the structures are fully optimized before further molecular dynamic (MD) calculations, and then we can obtain $L_0 \approx 20$ nm.

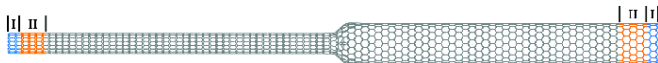


FIG. 1: (Color online). A typical $(n, 0)/(2n, 0)$ structure. Here, $n = 8$, and the number of pentagon-heptagon defects is $m = 4$. The regions marked as ‘I’ are fixed in MD process. The regions marked as ‘II’ are put in the heat baths.

In this kind of structure, the outmost one period of each heads (colored by blue and marked as region ‘I’ in Fig. 1) are fixed in MD process. Then two periods of each ends (illustrated by orange color and marked as region ‘II’ in Fig. 1) are put in the heat baths, which are realized by the Nosé-Hoover thermostat.³⁶ The temperatures of the thermostats at left and right heads are T_L and T_R , respectively. For convenient, here we introduce two quantities: $\Delta T = \frac{T_L - T_R}{2}$, and $\langle T \rangle = \frac{T_L + T_R}{2}$. In this work, $\langle T \rangle$ is always kept at 290 K.

The C-C bonding interactions are described by the second-generation reactive empirical bond order (REBO) potential,³⁷ which is the most recent version of the Tersoff-Brenner type potential, combining advantages of the two sets of parameters in the earlier version.³⁸

The velocity Verlet method is employed to integrate the equations of motion with the time step of 0.51 fs. The typical total MD process is 5×10^6 steps, which is about 2.55 ns, and the statistic averages of interesting quantities start from half of the MD process, i.e., 2.5×10^6 steps are used to relax the system to a stationary state.

The instant temperature of atoms i is defined as $T_i(t) = \frac{m_i}{3k_b} (v_x(t)^2 + v_y(t)^2 + v_z(t)^2)$, where $v(t)$ is the time-dependent velocity, m_i the mass and k_b the Boltzmann constant. This is a result of energy equipartition theorem.

The thermal flux is obtained from the thermostats, i.e., the total work from the thermostats can be regarded as the heat flux runs from thermostats to the system. If the work is positive, then the heat flux is also positive. In the scheme of the Nosé-Hoover thermostat,³⁶ the equation of motion for the particle i in heat bath is:

$$\dot{\vec{p}}_i = -\xi \vec{p}_i + \vec{f}_i, \quad \dot{\xi} = \frac{1}{Q} \left(\frac{\vec{p}_i \cdot \vec{p}_i}{m_i} - g k_b T \right), \quad (1)$$

where \vec{p}_i is the momentum and \vec{f}_i is the force applied on the atom. g is the number of degrees of freedom of the atoms in the thermostat. $Q = g k_b T \tau^2$, where τ is the relaxation time. In our simulation, τ is kept as 4 ps. The heat bath acts on the particle with a force $-\xi \vec{p}_i$, thus the power of heat bath is $-\xi \frac{\vec{p}_i \cdot \vec{p}_i}{m_i}$, which can also be regarded as the heat flux from heat bath, i.e.,

$$J_i = -\xi \frac{\vec{p}_i \cdot \vec{p}_i}{m_i}. \quad (2)$$

The total heat flux from the heat bath to the system can be obtained by $J = \sum_i J_i$, where the subscript i runs over all the particles in the thermostat. The final thermal conduction is $\kappa \cdot s = \frac{j \cdot s}{2\Delta T/L} = \frac{JL}{2\Delta T}$, where j is the heat flux density, s the area of cross-section, and L the system length. In fact this definition is equivalent to the usual definition: $J = \frac{d}{dt} \sum_i \vec{r}_i(t) \varepsilon_i(t)$, $\varepsilon_i(t)$ is the instant total energy of particle i , but Eq. (2) is much simpler for computational simulation.

III. NUMERICAL RESULTS AND DISCUSSIONS

First of all, we investigate the effect of defects in connection region. The defects in connection region determine the property of the interface between two tubes, and as a result, they will affect the heat transport property of the system. However, the question whether they can affect the rectification is still open.

We study the $(8, 0)/(16, 0)$ structures as examples.

Generally speaking, there are many methods to connect an IMJ, thus we only consider two conditions here. The first one is the coaxial straight IMJs. The possible number m of pentagon-heptagon defect pairs for a coaxial IMJ is 8, 4 or 2, but $m = 2$ makes the cross-section of the tube part highly deformed from circle, so we only consider $m = 4$ and 8. The second condition is the simplest IMJ, i.e., two tubes are connected with each other by using only one pair of heptagon-pentagon defects ($m = 1$).³⁹ The top views and side view of the three structures ($m = 8, 4$ and 1) are plotted in Fig. 2. It can be found even in the simplest zigzag/zigzag IMJ ($m = 1$), there is still a small angle between the two segments.

The total heat fluxes J versus the normalized temperature difference $\Delta T/\langle T \rangle$ is plotted in Fig. 3a. Positive

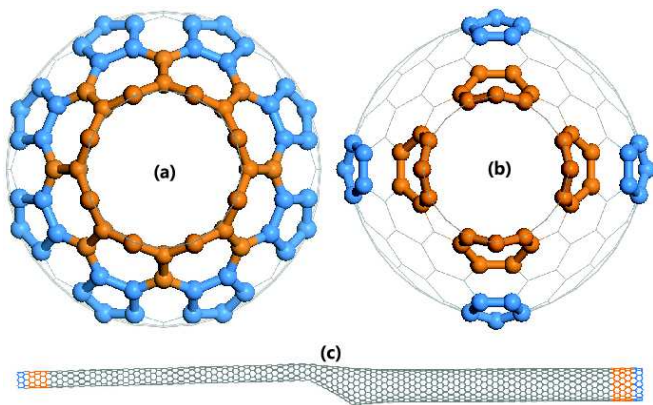


FIG. 2: (Color online). The top views and side view of two $(8, 0)/(16, 0)$ IMJs with different connection methods. (a) With 8 pairs of pentagon-heptagon defects. (b) With 4 pairs of pentagon-heptagon defects. (c) With only one pair of pentagon-heptagon defects.

J means the heat flux flows from $(n, 0)$ tube to $(2n, 0)$ tube. We do not show the heat flux density here, because it is difficult to define the area of the cross-section of the whole IMJ.

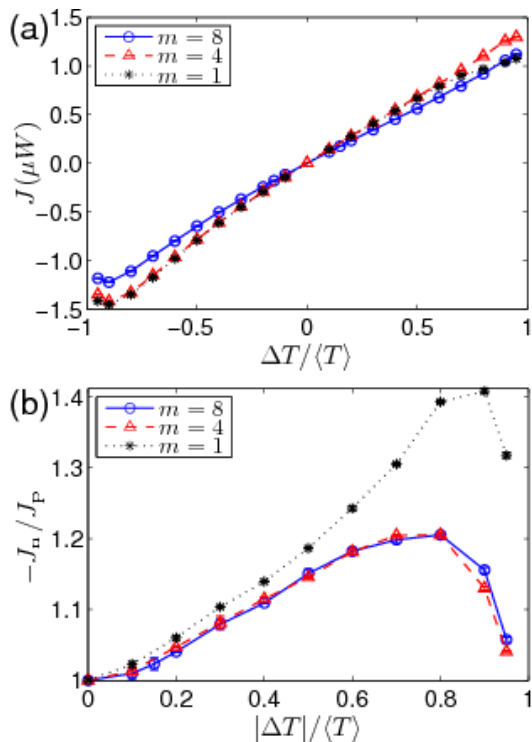


FIG. 3: (Color online). The thermal transports of $(8, 0)/(16, 0)$ SWCNT IMJs with different numbers of pentagon-heptagon defects in the connection region. (a) The heat flux versus temperature difference. (b) The thermal rectification versus temperature difference. m is the number of pentagon-heptagon defects. Error bars are also plotted.

It can be found from Fig. 3a that the total heat flux

for $m = 4$ is larger than that for $m = 8$. It is straightforward because the pentagon-heptagon defects are topological defects, they scatter the phonons and cause larger interfacial thermal resistance. As a result, more topological defects will reduce the thermal conductance and the heat flux. But the total heat flux for $m = 1$ is close to that for $m = 4$. This is due to the big difference of the connecting region of these IMJs. The length of the connecting region in IMJ with $m = 1$ is much longer than those in the IMJs with $m = 4$ or 8 . The long connecting region can cause big thermal resistance, as a result, the thermal resistance in $m = 1$ IMJ is not much smaller than that in $m = 4$ IMJ.

When the temperature difference is very small, the heat flux only shows weak asymmetry. The asymmetry becomes larger when temperature difference is larger. This characteristic is seen clearer in Fig. 3b, in which the thermal rectification $|J_n/J_p| = -J_n/J_p$ is drawn.

In Fig. 3b, J_n means that the heat flux is of negative sign, *vice versa*, J_p means that the heat flux is of positive sign. It can be seen that, an increase in temperature gradient $|\Delta T|$ leads to an increase of thermal rectification. This is because the rectification is a result of non-equilibrium transport, which is mainly determined by optical phonons. Only when the temperature difference is large enough, the optical phonons can be excited and contribute to the heat conduction. More interestingly, when the temperature difference is large enough (for $|\Delta T| \approx 0.8\langle T \rangle$), the rectification begins to decrease. But, the temperature difference is so large that this result may not be hold in more restrict calculations due to lose of local thermal equilibrium and the quantum effect in the lower temperature head. Another meaningful feature is that, although the absolute values of the heat fluxes are completely different, rectifications are almost the same in IMJs with $m = 4$ and 8 , whose connecting region is short. Namely, the rectification is weakly dependent on the detailed structure of the interface when the connecting region is short enough. And the rectification in $m = 1$ IMJ is largest among the three kinds IMJs.

In order to understand above rectification phenomenon, we consider the power spectra of the atoms around the connecting part. The atoms to be studied are illustrated in the Fig. 4a. They are selected to be next to the defects along the axes. The corresponding phonon spectra are presented in the Fig. 4b. And the overlapping of the phonon spectra of the two atoms around the connecting parts have been emphasized by shadows.

It is found that when the direction of the temperature gradient is exchanged, the area of the overlap region is also changed. More importantly, the overlap area is larger when $\Delta T/\langle T \rangle$ is negative. This result corresponds with the trend of the heat flux. So we can state that in this real system, the relationship between the overlap area and the absolute value of the heat flux is same as that in the one dimensional nonlinear lattice systems^{2,3,4}, in which it is found that matching/mismatching of the en-

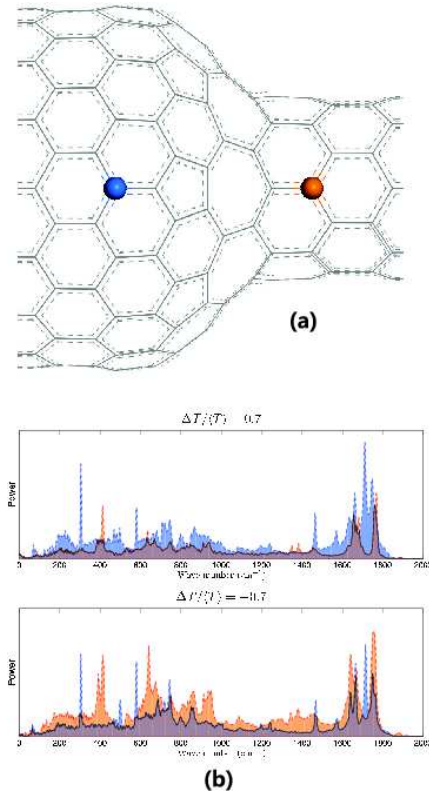


FIG. 4: (Color online). (a) The side view of the (8, 0)/(16, 0) IMJ ($m = 8$), where the atoms whose power spectra are recorded are emphasized by balls. (b) The corresponding phonon power spectra. The overlapping of the phonon spectra of the two particles around the connecting parts have been emphasized by shadows and bordered by dark lines.

ergy spectra around the interface is the underlying mechanism of the rectification.

On the other hand, the most obvious change appears at $400\sim 1000\text{ cm}^{-1}$ and $1600\sim 1800\text{ cm}^{-1}$. The $m = 4$ IMJ is also studied, and similar conclusion can be obtained. So the optical phonon modes are important for the rectification. In addition, in Ref. 35, the authors show that in carbon nanotubes with finite length where the long-wavelength acoustic phonons behave ballistically, even optical phonons can play a major role in the non-Fourier heat conduction. The dispersion relations of the SWNT show that, in the intermediate range of the normalized wave vector $0.1 < k^* < 0.9$, some of the phonon branches, especially the ones with relatively low frequency, have group velocity comparable to the acoustic branches.

Furthermore, the thermal conductivity can be expressed as $\kappa = \sum_q l_{\lambda q} C_q(\omega_\lambda) v_{\lambda q}$, where λ is a set of quantum numbers specifying a phonon state, l is the phonon mean free path, $v_{\lambda q}$ is the magnitude of the phonon group velocity along the direction of the heat flow, and $C_q(\omega) = k_B \left(\frac{\hbar\omega}{k_B T}\right)^2 \frac{\exp(\hbar\omega/k_B T)}{[\exp(\hbar\omega/k_B T) - 1]^2}$ is the thermal capacity of lattice wave with wave vector q and angular frequency ω . Thus, the contribution from the high fre-

quency modes is weak because their group velocities are much smaller than those of low frequency modes. So the modes at $400\sim 1000\text{ cm}^{-1}$ are more important than the modes at $1600\sim 1800\text{ cm}^{-1}$.

The frequencies of the low frequency modes have been found to be inversely proportional to the tube radius.⁴⁰ Thus, the low frequency modes, e.g., the radial breathing mode, have different exciting temperatures in (16, 0) and (8, 0) tubes. On the other words, their participation in transport process occurs at different temperatures. This fact further explains why these low frequency optical phonon modes are important for the rectification.

Based on above discussions, now we can understand the following phenomena. Firstly, the rectification almost does not change in the $m = 4$ and 8 IMJs. Secondly, the rectification in $m = 1$ IMJ is largest in the three IMJs.

As has been mentioned, the modes at $400\sim 1000\text{ cm}^{-1}$ are most important for the thermal rectification. These modes have larger wave lengths than the high frequency modes. The connecting parts of the two IMJs with $m = 4$ and 8 are short, as a result, the defects have weak effect on the effective optical modes. In Ref. 41, it is found that the high frequency vibrational modes caused by topological defects are localized states. And the higher frequency localized modes show smaller spatial dimension, which means they can hardly entangle with the transport phonon modes. Thus in the short connecting IMJs ($m = 4$ and 8), the arrangement of the detailed defects has weak influence on the rectification. In contrast, the connecting region is much longer in the $m = 1$ IMJ, and the distance between the pentagon and heptagon rings is relatively long, which means the connecting region can affect those middle frequency phonon modes, which have longer wave lengths. Therefore, the rectification is largest in the case of $m = 1$ IMJ.

However, the rectification in current structures is still small, which might limit the application of the IMJ as a thermal rectifier. So we will try to find the factors which can help improve the rectification.

Above all, we investigate the thermal conductance of the IMJs with the different index n numerically.

In order to make the results comparable with each other, the number m of pentagon-heptagon defect pairs are set to be n . Considering the computational consumption, only $n = 7, 8$ and 9 are considered in Fig. 5.

According to Fig. 5a, the total heat flux increases when n increases, but this does not mean that the thermal conductivity for big n is also large because it should be scaled by the area of cross-section. In fact, it has been shown that the thinner SWCNTs have higher thermal conductivity in literatures.^{15,18,23}

Another interesting feature is that, when index n increases, the asymmetric heat flux ratio does not always increase. In Fig. 5b, the largest rectification appears when $n = 8$. So this reminds us that the heat flux rectification is not only induced by the radius difference of two segments. When tube radius increases to a sufficient large value, i.e., n is large, the vibrational density

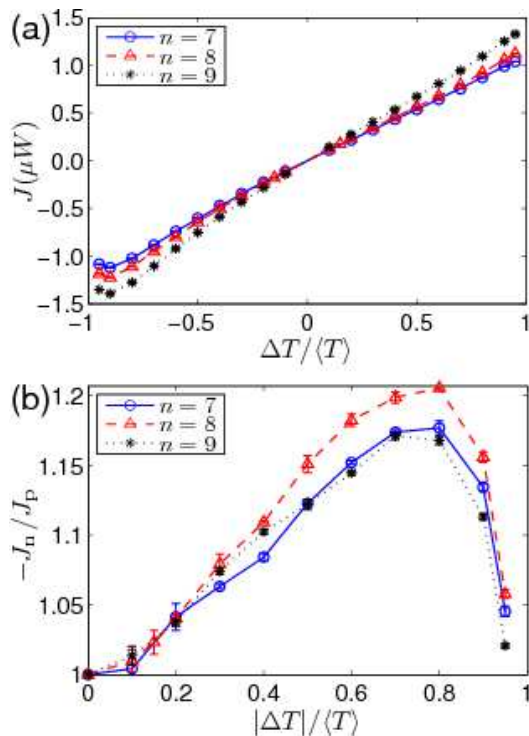


FIG. 5: (Color online). The thermal transports of $(n, 0)/(2n, 0)$ SWCNT IMJs, $n = 7, 8$ and 9 . (a) The heat flux versus temperature difference. (b) The thermal rectification versus temperature difference. In this figure, $m = n$. Error bars are also plotted.

of states (VDOS) of carbon nanotube approaches to that of the graphite. But when n is small, the VDOS of the SWNT deviates from that of the graphite due to the periodical boundary along the circumferential direction and the curvature effect, and the amplitude of the deviation is almost inversely proportion to n . As a result, when $(n, 0)$ and $(2n, 0)$ tubes connect with each other, the difference between the VDOSs of the two tubes is obvious if n is small, and *vice versa*, the difference is not so obvious if n is large. Recalling the fact that the rectification can be related with the mismatching between the VDOSs around the connecting region, we can conclude that the rectification of the IMJ is not obvious when n is large.

Next, we investigate the length dependence of heat conduction. From Fig. 6a, it can be seen that the total heat flux decreases as the system length increases from L_0 to $2L_0$. However, the thermal conductivity, $\kappa = \frac{JL}{2s\Delta T}$, increases with the increasing of the system length. This result agrees with the previous studies. Moreover, there still exists asymmetry in the heat flux, which is clearly illustrated in Fig. 6b. Where the rectification at different $|\Delta T|$ is plotted for different system lengths. Obviously, the increase of system length weakens rectification. It can be understood as follows. As the system length increases, long-wave phonons modes contribute more to the heat conduction. This kind of heat conduction is symmetric because long-wave phonon modes are hardly scat-

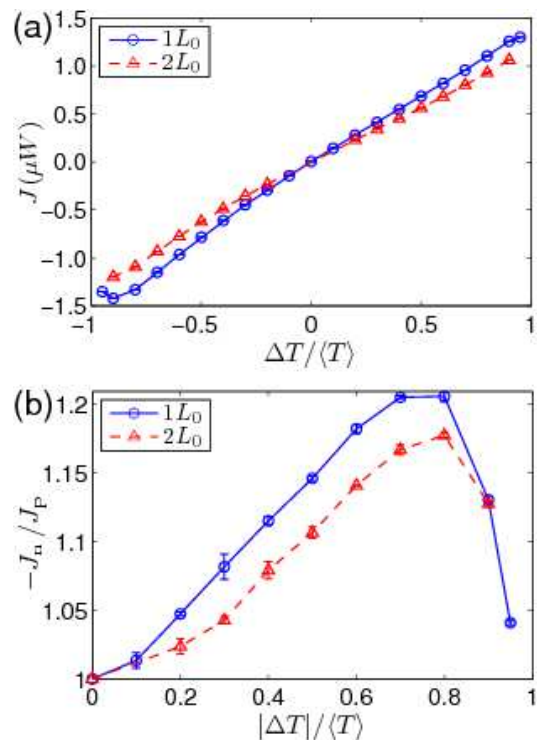


FIG. 6: (Color online). The thermal transports of $(8, 0)/(16, 0)$ SWCNT IMJs with different length. (a) The heat flux versus temperature difference. (b) The thermal rectification versus temperature difference. $m = 4$. L_0 is defined in text. Error bars are also plotted.

tered by the junction or any local defects. Moreover, the asymmetric thermal conductance is mainly controlled by the asymmetric interface, i.e., the connection part, which does not change when system length increases. As a result, although the absolute value does not change, the rectification appears to be smaller.

Based on above study, we can conclude that changes in radial and axial direction have different influence on rectification. The increase of structural asymmetry around the interface can increase the rectification. In the following section we will discuss other alternatives to improve the rectification.

IV. IMPROVEMENT

First, it is possible to increase the difference in force constants around the interface by applying external stress. Because the Young's modulus has been proved to be almost the same in different tubes using the Tersoff-Brenner potential,⁴² it can be expected that the $(n, 0)$ tube and $(2n, 0)$ tube will give different response to the same external stress. Thus it is possible that one can use this property to fabricate devices. Here we consider two kinds of stresses, tensile and torsional stresses. It has been proven in the framework of tight-binding⁴³ that these two stresses can change the electronic structure of

SWCNTs greatly. Here the (8, 0)/(16, 0) SWCNT IMJ ($m = 4$) is taken as an example. The original length is L_0 .

The stresses considered in this work are all small enough to ensure the system does not undergo any structural transformations⁴⁴ or defects.⁴⁵ For tensile stress, we elongate the IMJ along the axial direction by 3%. For torsional stress, one head of IMJ is rotated relative to the other by 30° around the axis. The results are shown in Fig. 7.

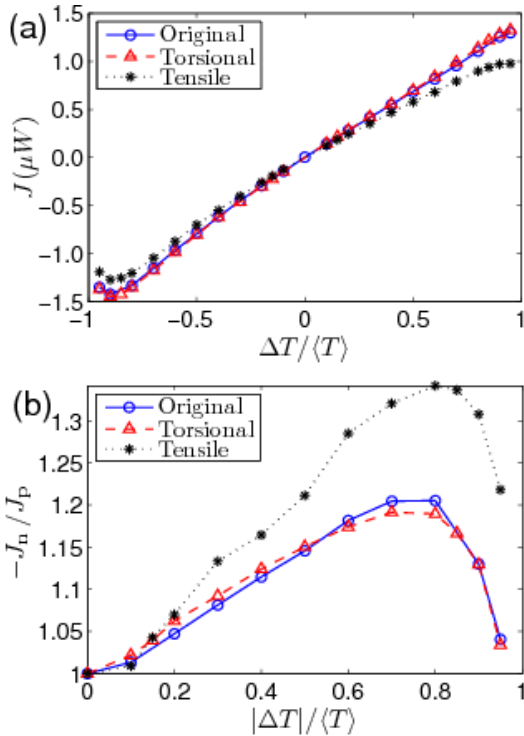


FIG. 7: (Color online). The thermal transports of (8, 0)/(16, 0) SWCNT IMJs under different stresses. (a) The heat flux for different stresses. (b) The thermal rectification for different stresses. $m = 4$. Error bars are also plotted.

It can be seen that the torsional deformation can change neither the absolute value of heat flux nor the asymmetric behavior largely. However, the tensile stress can greatly change the heat transport. In the elongated structure, the heat flux becomes smaller than that of undeformed structure, but the rectification becomes larger.

Above results are reasonable. First of all, the deformation of the thicker tube is smaller than that of thinner ones under same external stress. This means that when thick and thin tubes are connected with each other to form IMJ, they will appear different axial deformation under the same stress, which will further increase the structural difference between the two tubes. Secondly, the heat transport in carbon nanotubes are mainly contributed by the four acoustic phonon modes. These phonon modes have weak dependence on the local structure, but they can be affected by the shape of the cylinder surface. When tensile stress is applied to the SWCNTs,

the SWCNTs will shrink in the radial direction and elongate in the axial direction. This means their cylinder surface will change, so that the acoustic phonon modes will also be changed. But when SWCNTs are twisted, the cylinder surface almost does not change, so that the thermal conductance almost does not change.

Comparing Fig. 7a and 3a, it can be found that the heat flux decreases in elongated structure. The reason is straightforward. As mentioned above, the thermal conductivity can be expressed as $\kappa = \sum_q l_{\lambda q} C_q(\omega_{\lambda}) v_{\lambda q}$,

where $C_q(\omega) = k_B \left(\frac{\hbar\omega}{k_B T} \right)^2 \frac{\exp(\hbar\omega/k_B T)}{[\exp(\hbar\omega/k_B T) - 1]^2}$. For the low frequency ($\hbar\omega \ll k_B T$) modes, which are most important for the thermal transport, $C_q(\omega) \approx k_B$. Furthermore, $l_{\lambda q}$ and $v_{\lambda q}$ are the increasing functions of the force constants k , thus the thermal conductivity κ is also an increasing function of the force constants k . In fact, some numerical simulations show that $\kappa \propto k^2$ in the weak coupled lattice models.^{2,46} When the system is elongated, the bonds along the axis are also elongated. Then according to the Abell-Tersoff formalism of the Tersoff-Brenner potential, the corresponding force constants will decrease. Finally, the thermal conductivity decreases in the elongated structure.

To elongate an IMJ is not very difficult for the state-of-the-art experiments, so we believe that tensile stress can be a possible method to improve the rectification.

Next, we will try to modify the structure to change rectification.

It is suggested^{2,3} that a suitable on-site potential can induce large rectification in two-segment model. So it is quite interesting that what will happen if some periodical potential is introduced into the SWCNT IMJs. On the other hand, a nanotube with sufficiently large diameter can be filled with spherical C_{60} fullerene molecules to build up a new hybrid structure referred to as a ‘peapod’,^{48,49} with spherical fullerenes representing peas and the carbon nanotube representing a pod. The thermal conductivity of the peapod structure has been investigated by using MD recently.⁵⁰ So it is possible to combine these two structures, i.e., IMJs and peapod, into a new structure.

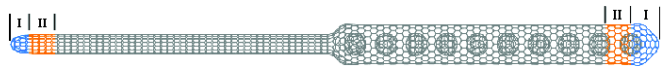


FIG. 8: (Color online). The (8, 0)/ C_{60} @(16, 0) structure. The number of pentagon-heptagon defects is $m = 4$. The regions marked as ‘I’ are fixed in MD process. The regions marked as ‘II’ are put in the heat baths.

The structure (see Fig. 8) contains two parts, i.e., a segment of $(n, 0)$ SWCNT and a segment of $(2n, 0)$ SWCNT with some C_{60} balls inserted into its center, which is typically called as SWCNT peapod structure. The lengths of these two segments are almost the same. They are connected by m pairs of pentagon-heptagon defects. Because the closest distances between the adjacent

C_{60} balls are almost same, 10.05 \AA , we can consider that they exert an external periodic potential on the outside SWCNT. Here, the interaction between two atoms on C_{60} balls and outside SWCNT is modeled by Lennard-Jones potential:

$$V(r) = 4\varepsilon \left[-\left(\frac{\sigma}{r}\right)^6 + \left(\frac{\sigma}{r}\right)^{12} \right], \quad (3)$$

with parameters, $\varepsilon = 2.964 \text{ meV}$ and $\sigma = 3.407 \text{ \AA}$. By default, the total length of the structure is L_0 , which permits 10 C_{60} balls in the $(2n, 0)$ segment.

In this complex structure, the two heads are closed to ensure the C_{60} balls not running out in the MD calculations. And several periods of two heads (presented by blue color and marked as region 'I' in Fig. 8) are fixed in the MD simulation. Then two periods of each ends (emphasized by orange color and marked as region 'II' in Fig. 8) are put in the Nosé-Hoover thermostat.³⁶

In Fig. 9, the heat transports of $(8, 0)/C_{60}@16, 0$ structure with different lengths are shown.

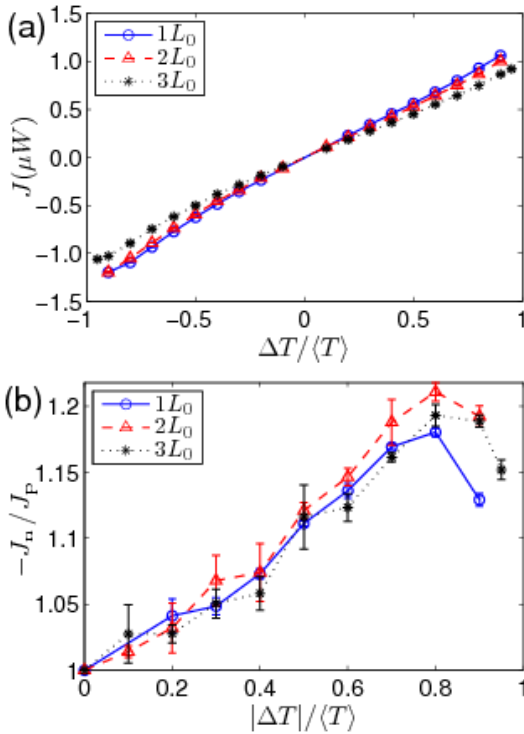


FIG. 9: (Color online). The thermal transports of $(8, 0)/C_{60}@16, 0$ structures with different length. (a) The heat flux versus temperature difference. (b) The thermal rectification versus temperature difference. $m = 4$. L_0 is defined in text. Error bars are also plotted.

Comparing Fig. 9a with Fig. 6a, one can find that the heat flux of peapod structure is smaller than that of the empty IMJ, which seems to be in contradict with the result in Ref. 50. But it should be pointed out that in our structure the peapod region is closed at the ends. In fact,

this prevents the possible mass transport (via fullerenes) which in turn reduces the assistance transport effect of C_{60} balls. Furthermore, because of the coupling between the phonon modes (mainly the radial breathing modes) of carbon nanotube (CNT) and C_{60} balls, the conduction phonon will be scattered and the thermal conductivity of outside CNT will be reduced.

On the other hand, we can notice that the length of error bars in Fig. 9b is much larger than that in Fig. 6b. This means that the existence of C_{60} balls increases the fluctuations in the heat flux. In Ref. 50, it is found that the temperature fluctuations of peapod structure are larger than that of empty nanotube. It is explained by the weak van der Waals forces between fullerenes and the outside CNT.

Another result is that the existence of C_{60} balls can hardly change the asymmetric behavior of heat flux. This is somehow disappointing for us, because it is natural to expect that the periodical potential introduced by the C_{60} balls can enhance the thermal rectification according to the results based on lattice models. However, our numerical results are also reasonable because of following facts. The periodical potential introduced by the C_{60} balls is intrinsically van der Waals potential, so its strength is much weaker than the binding potential among the carbon atoms in SWCNT. The period of the periodical potential introduced by C_{60} balls is about 10 \AA , which is too large compared with the C-C bond length in SWCNT, thus only low frequency vibrational phonons are affected. As has been mentioned, the asymmetric heat flux is controlled by the optical phonon modes, so the change of low frequency vibrational modes can hardly change the asymmetric behavior.

According to our result, if one wants to build a thermal rectifier by applying periodical external potential, van der Waals force is not a good choice.

V. CONCLUSIONS

In this work, heat rectification in $(n, 0)/(2n, 0)$ IMJs has been studied. It is found that the rectification depends weakly on the detailed structure of connection part, but depends strongly on the temperature gradient. The rectification increases as the temperature gradient increases.

We have also studied the dependencies of the rectification on tube radius and IMJ length. We found that the maximum rectification appears in short $(8, 0)/(16, 0)$ IMJ.

Moreover, we have found that the tensile stress can increase the rectification, while torsional stress can not. It is due to the different effects of the stresses on IMJ structure. It can be believed that the tensile stress will play an important role in building of devices with highly asymmetric transport behavior.

The 'peapod' structure is combined with IMJ structure to investigate the effect of periodical potential on the

rectification. Our numerical result shows that the new structure can hardly change the rectification.

The study may shed lights in further experimental investigation in this field.

Acknowledgments

This work is supported in part by an academic research fund of MOE, Singapore, and the DSTA under Project

Agreement No. POD0410553.

-
- * Electronic address: wugaxp@gmail.com
 † Corresponding author. Electronic address: phylbw@nus.edu.sg
- ¹ F. Bonetto, J. L. Lebowitz, and L. Rey-Bellet, In *Mathematical Physics 2000*, edited by A. Fokas, A. Grigoryan, T. Kibble, and B. Zegarlinsky (Imperial College Press, London, 2000) pp. 128-150; S. Lepri, R. Livi, and A. Politi, *Phys. Rep.* **377**, 1 (2003); B. Li, J. Wang, L. Wang, and G. Zhang, *Chaos* **15**, 015121 (2005).
 - ² B. Li, L. Wang, and G. Casati, *Phys. Rev. Lett.* **93**, 184301 (2004).
 - ³ B. Li, J.H. Lan, and L. Wang, *Phys. Rev. Lett.* **95**, 104302 (2005).
 - ⁴ J. H. Lan and B. Li, *Phys. Rev. B* **74**, 214305 (2006); J. H. Lan and B. Li, *Phys. Rev. B* **75**, 214302 (2007).
 - ⁵ N. Yang, N.- B Li, L Wang, and B Li, *Phys. Rev. B* **76**, 020301(R) (2007).
 - ⁶ B. Li, L. Wang, and G. Casati, *Appl. Phys. Lett.* **88**, 143501 (2006).
 - ⁷ C. W. Chang, D. Okawa, A. Majumdar, and A. Zettl, *Science* **314**, 1121 (2006).
 - ⁸ D. G. Cahill, W. K. Ford, K. E. Goodson, G. D. Mahan, A. Majumdar, H. J. Maris, R. Merlin, and S. R. Phillpot, *J. Appl. Phys.* **93**, 793(2003).
 - ⁹ J.W. Che, T. Cagin, W.A. Goddard, *Nanotechnology* **11**, 65 (2000).
 - ¹⁰ S. Maruyama, *Physica B* **323**, 193 (2002); S. Maruyama, *Microscale Thermophysical Engineering* **7**, 41 (2003).
 - ¹¹ W. Zhang, Z.Y. Zhu, F. Wang, T.T. Wang, L.T. Sun, and Z.X. Wang, *Nanotechnology* **15**, 936 (2004).
 - ¹² N.G. Mensah, G. Nkrumah, S.Y. Mensah, and F.K.A. Alotey, *Phys. Lett. A* **329**, 369 (2004).
 - ¹³ Z. Yao, J.S. Wang, B. Li, and G.R. Liu, *Phys. Rev. B* **71**, 085417 (2005).
 - ¹⁴ N. Mingo and D.A. Broido, *Nano Lett.* **5**, 1221 (2005); N. Mingo and D.A. Broido, *Phys. Rev. Lett.* **95**, 096105 (2005).
 - ¹⁵ G. Zhang and B. Li, *J. Phys. Chem. B* **109**, 23823 (2005).
 - ¹⁶ M. Grujicic, G. Cao, and W.N. Roy, *J. Materials Science* **40**, 1943 (2005).
 - ¹⁷ J. S. Wang, J. Wang and N. Zeng, *Phys. Rev. B* **74**, 033408 (2006).
 - ¹⁸ J. Wang and J.S. Wang, *Appl. Phys. Lett.* **88**, 111909 (2006).
 - ¹⁹ J. Hone, M. Whitney, C. Piskoti, and A. Zettl, *Phys. Rev. B* **59**, R2514 (1999).
 - ²⁰ S. Berber, Y.K. Kwon, and D. Tomanek, *Phys. Rev. Lett.* **84**, 4613 (2000).
 - ²¹ P. Kim, L. Shi, A. Majumdar, and P.L. McEuen, *Phys. Rev. Lett.* **87**, 215502 (2001).
 - ²² C.H. Yu, L. Shi, Z. Yao, D.Y. Li, and A. Majumdar, *Nano Lett.* **5**, 1842 (2005).
 - ²³ M. Fujii, X. Zhang, H.Q. Xie, H. Ago, K. Takahashi, T. Ikuta, H. Abe, and T. Shimizu, *Phys. Rev. Lett.* **95**, 065502 (2005).
 - ²⁴ E. Pop, D. Mann, Q. Wang, K. Goodson, and H.J. Dai, *Nano Lett.* **6**, 96 (2006).
 - ²⁵ T. Y. Choi, D. Poulidakos, J. Tharian, and U. Sennhauser, *Nano Lett.* **6**, 1589 (2006).
 - ²⁶ G. Zhang and B. Li, *J. Chem. Phys.* **123**, 014705(2005); C. W. Chang, A. M. Fennimore, A. Afanasiev, D. Okawa, T. Ikuno, H. Garcia, Deyu Li, A. Majumdar, and A. Zettl, *Phys. Rev. Lett.* **97**, 085901 (2006).
 - ²⁷ B. I. Dunlap, *Phys. Rev. B* **49**, 5643 (1994).
 - ²⁸ J.-C. Charlier, T.W. Ebbesen, and Ph. Lambin, *Phys. Rev. B* **53**, 11 108 (1996).
 - ²⁹ L. Chico, V. H. Crespi, L. X. Benedict, S. G. Louie, and M. L. Cohen, *Phys. Rev. Lett.* **76**, 971 (1996).
 - ³⁰ R. Saito, G. Dresselhaus, and M. S. Dresselhaus, *Phys. Rev. B* **53**, 2044 (1996).
 - ³¹ V. Meunier, P. Senet, and Ph. Lambin, *Phys. Rev. B* **60**, 7792 (1999).
 - ³² M. S. Ferreira, T. G. Dargam, R. B. Muniz, and A. Latgé, *Phys. Rev. B* **62**, 16040 (2000).
 - ³³ L.F. Yang, J.W. Chen, H.T. Yang, and J.M. Dong, *Euro. Phys. J. B* **33** (2), 215 (2003).
 - ³⁴ J. Han, M. P. Anantram, R. L. Jaffe, J. Kong and H. Dai, *Phys. Rev. B* **57**, 14983 (1998).
 - ³⁵ J. Shiomi and S. Maruyama, *Phys. Rev. B* **73**, 205420 (2006).
 - ³⁶ S. Nose, *J. Chem. Phys.* **81**, 511 (1984); W. G. Hoover, *Phys. Rev. A* **31**, 1695 (1985).
 - ³⁷ D.W. Brenner, O.A. Shenderova, J. A. Harrison, S. J. Stuart, B. Ni, and S. B. Sinnott, *J. Phys.: Condens. Matter* **14**, 783 (2002).
 - ³⁸ D.W. Brenner, *Phys. Rev. B* **42**, 9458 (1990).
 - ³⁹ R. Saito, G. Dresselhaus, and M.S. Dresselhaus, *Physical Properties of Carbon Nanotubes* (London: Imperial College Press, 1998).
 - ⁴⁰ R. Saito, T. Takeya, T. Kimura, G. Dresselhaus, and M.S. Dresselhaus, *Phys. Rev. B* **57**, 4145 (1998).
 - ⁴¹ G. Wu and J. Dong, *Phys. Rev. B* **73**, 245414 (2006).
 - ⁴² A. Sears and R.C. Batra, *Phys. Rev. B* **69**, 235406 (2004).
 - ⁴³ L. Yang, M. P. Anantram, J. Han, and J. P. Lu, *Phys. Rev. B* **60**, 13 874 (1999); L. Yang and J. Han, *Phys. Rev. Lett.* **85**, 154 (2000).

- ⁴⁴ B. I. Yakobson, C.J. Brabec, and J. Bernholc, Phys. Rev. Lett. **76**, 2511 (1996).
- ⁴⁵ M.B. Nardelli, B.I. Yakobson, and J. Bernholc, Phys. Rev. Lett. **81**, 4656 (1998).
- ⁴⁶ K. R. Patton and M. R. Geller, Phys. Rev. B **64**, 155320 (2001); B. Hu, D.He, L. Yang and Y. Zhang, Phys. Rev. E **74**, R060101 (2006).
- ⁴⁷ B. Hu, L. Yang, and Y. Zhang, Phys. Rev. Lett. **97**, 124302 (2006).
- ⁴⁸ B.W. Smith, M. Monthieux, and D.E. Luzzi, Nature (London) **396**, 323 (1998).
- ⁴⁹ S. Okada, S.Saito, and A. Oshiyama, Phys. Rev. Lett. **86**, 3835 (2001).
- ⁵⁰ E.G. Noya, D. Srivastava, L.A. Chernozatonskii, and M. Menon, Phys. Rev. B **70**, 115416 (2004).